

All-Optical Molecular Orientation

Keita Oda, Masafumi Hita, Shinichirou Minemoto, and Hirofumi Sakai*

Department of Physics, Graduate School of Science, The University of Tokyo, 7-3-1 Hongo, Bunkyo-ku, Tokyo 113-0033, Japan
(Received 18 September 2009; published 24 May 2010)

We report clear evidence of all-optical orientation of carbonyl sulfide molecules with an intense nonresonant two-color laser field in the adiabatic regime. The technique relies on the combined effects of anisotropic hyperpolarizability interaction and anisotropic polarizability interaction and does not rely on the permanent dipole interaction with an electrostatic field. It is demonstrated that the molecular orientation can be controlled simply by changing the relative phase between the two wavelength fields. The present technique brings researchers a new steering tool of gaseous molecules and will be quite useful in various fields such as electronic stereodynamics in molecules and ultrafast molecular imaging.

DOI: 10.1103/PhysRevLett.104.213901

PACS numbers: 42.65.Ky, 32.80.Rm, 42.50.Hz

Since most molecules are anisotropic quantum systems, alignment and orientation dependence in various experiments using molecules as a sample are always a matter of central concern. The molecular alignment techniques [1,2] are relatively well developed and have greatly contributed to progress in studies on the alignment dependence of multiphoton ionization [3–5], structural deformation [6], and high-order harmonic generation [7–9]. Nowadays, researchers are turning their attention to molecular orientation, which is generally thought to be much more challenging than molecular alignment. In the existing molecular orientation techniques, an electrostatic field has always been required to determine the head-versus-tail order. Traditional techniques are brute-force orientation [10,11] and hexapole focusing [12]. By brute-force orientation, some particular molecules with large permanent dipole moments can be oriented in a very high electrostatic field. An inhomogeneous electrostatic field created by the hexapole focuser can be used to orient state-selected (near) symmetric top molecules. Modern techniques for molecular orientation are based on the combined electrostatic and intense nonresonant laser fields [13]. Our group has demonstrated both one- [14,15] and three-dimensional molecular orientation [16] with a linearly and elliptically polarized laser field, respectively, in the presence of a weak electrostatic field. More recently, we have even achieved laser-field-free molecular orientation by rapidly truncating an intense laser field at its peak intensity in a weak electrostatic field [17,18]. In the existing techniques relying on the permanent dipole interaction with an electrostatic field, the spatial direction of molecular orientation is determined by the electrostatic field created by the space-fixed electrodes, and virtually nonpolar asymmetric molecules cannot be oriented.

As an alternative approach to achieve molecular orientation without an electrostatic field, we have proposed a novel technique with an intense, nonresonant, two-color laser field [19]. Among various proposals [19–23] to achieve molecular orientation with a two-color laser field,

ours [19] is the only technique which relies neither on the permanent dipole interaction nor on a resonant process. In this Letter we demonstrate all-optical molecular orientation with an intense nonresonant two-color laser field. The form of a two-color, linearly polarized, phase-locked laser electric field is expressed as

$$E(t) = E_{\omega}(t) \cos \omega t + E_{2\omega}(t) \cos(2\omega t + \phi), \quad (1)$$

with $E_{\omega}(t)$ and $E_{2\omega}(t)$ the electric field amplitude profiles of the ω and 2ω fields, respectively, and ϕ the phase difference between the two wavelengths. After the cycle average of the rapid oscillation of the laser electric field, the total Hamiltonian of a linear molecule interacting with the asymmetric field [Eq. (1)] is given by

$$H(t) = B\mathbf{J}^2 - \frac{1}{4}(\alpha_{zz} \cos^2 \theta + \alpha_{xx} \sin^2 \theta)[E_{\omega}^2(t) + E_{2\omega}^2(t)] - \frac{1}{8}(\beta_{zzz} \cos^3 \theta + 3\beta_{zxx} \cos \theta \sin^2 \theta) \cos \phi E_{\omega}^2(t) E_{2\omega}(t), \quad (2)$$

with B the rotational constant of the molecule, \mathbf{J}^2 the squared angular momentum operator, θ the angle between the laser polarization and the molecular axis, α_{zz} and α_{xx} the polarizability components parallel and perpendicular to the molecular axis, respectively, and β_{zzz} and β_{zxx} the hyperpolarizability components parallel and perpendicular to the molecular axis, respectively. The Hamiltonian [Eq. (2)] explains the underlying mechanism of the present molecular orientation technique. The double-well potential is created mainly by the anisotropic polarizability interaction given by the second term in Eq. (2) and the asymmetry in the potential is brought by the anisotropic hyperpolarizability interaction given by the third term in Eq. (2). It should be noticed that the permanent dipole interaction vanishes in Eq. (2) after the cycle average. Since the permanent dipole interaction does not play any role, the present technique can also be applied to orient virtually nonpolar asymmetric molecules as discussed below.

A schematic diagram of the experimental setup is shown in Fig. 1. The two-color, linearly polarized, phase-locked

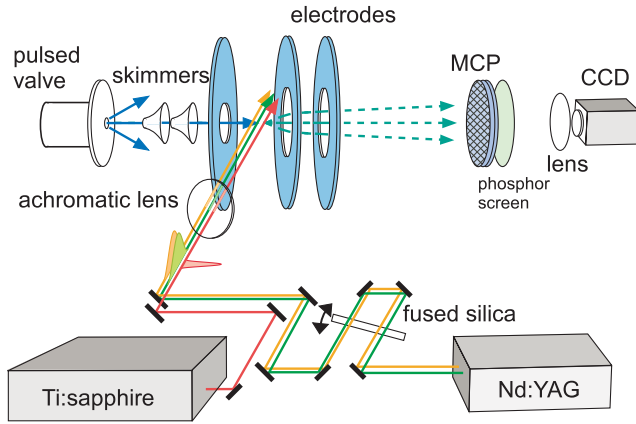


FIG. 1 (color online). A schematic diagram of the experimental setup. The illustrations of the two-color pump and the probe pulses depict their polarization directions.

laser electric field is formed by the superposition of the fundamental pulse (wavelength $\lambda_\omega = 1064$ nm) from an injection-seeded nanosecond Nd:YAG laser (pulse width $\tau \sim 12$ ns) and its second harmonic pulse ($\lambda_{2\omega} = 532$ nm). The pulse width of 12 ns ensures that molecular orientation proceeds adiabatically. The relative phase between the two wavelengths is controlled by the rotation of a 6.35-mm-thick fused silica plate. The two wavelengths are collinearly focused into the vacuum chamber by a 250-mm-focal-length plano-convex achromatic lens. The typical intensity is $I \sim 1 \times 10^{12}$ W/cm² for each wavelength. With these intensities for the two-color pump pulse, we confirm that the ionization of carbonyl sulfide (OCS) molecules is negligible. The sample is OCS molecules 5% diluted with Ar, which is supplied as a supersonic molecular beam by a pulsed valve equipped with a 0.25-mm-diam nozzle. The stagnation pressure is 10 atm. After passing through two 0.5-mm-diam skimmers, the OCS molecular beam enters the interaction region and is crossed at right angles with the two-color pump pulse. The molecular orientation is probed by observing fragment ions produced from multiply ionized molecules with the velocity map ion imaging technique. An intense femtosecond probe pulse ($\lambda \sim 800$ nm, $\tau \sim 100$ fs, $I \sim 3 \times 10^{14}$ W/cm²) is collinearly focused into the vacuum chamber with the two-color pump pulse and is used to multiply ionize the molecules at the peak of the two-color pump pulse. The two-dimensional ion detector consists of a microchannel plate and a phosphor screen. The ion image on the phosphor screen is recorded by a charge-coupled-device camera. The polarizations of the two-color pump and the probe pulses are parallel and perpendicular to the detector plane, respectively.

Figure 2 shows typical two-dimensional ion images for CO⁺ and S⁺ fragments. The center parts of the images are saturated due to the intense ion signals, which are not the focus of the present study and consist of background molecular ions N₂⁺ (O₂⁺) with the same mass to charge ratio as that of CO⁺ (S⁺) and the fragment ions with low

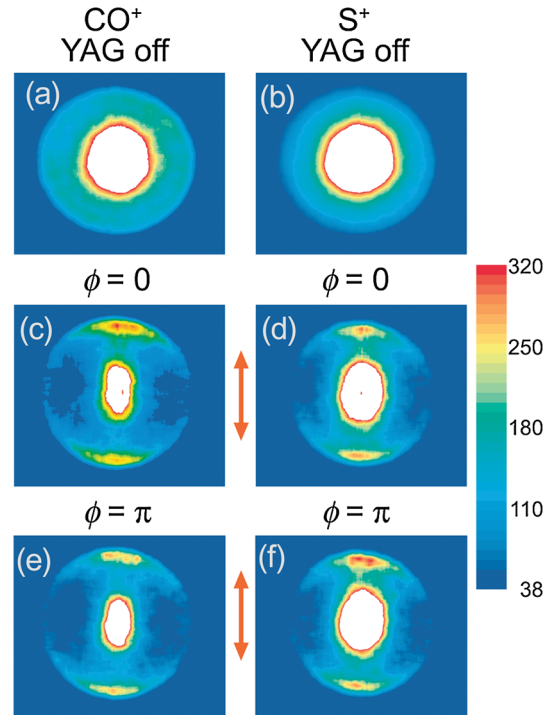


FIG. 2 (color). Typical two-dimensional ion images for CO⁺ (left column) and S⁺ (right column) fragments. The images in the top panel [(a) and (b)] are obtained without the two-color laser field. The images in the middle [(c) and (d)] and bottom [(e) and (f)] panels are obtained when the two-color laser field is applied with the relative phase of zero and pi, respectively. The polarizations of the two-color laser field are shown by the arrows.

released kinetic energy produced from OCS⁺. Here we concentrate on the fragment ions distributed in the outer rings. Those fragment ions with high released kinetic energy are preferentially produced from OCS²⁺. Since the dissociation takes place very rapidly, the emitted directions of the fragment ions are considered to reflect the directions of the molecular axes just before dissociation. The images in the top panel [Figs. 2(a) and 2(b)] are obtained without the two-color laser field. Both CO⁺ and S⁺ images look center-symmetric, allowing us to interpret that the OCS molecules are randomly oriented.

When the two-color phase-locked laser field is applied with the polarizations shown by the arrows in Figs. 2(c)–2(f), the fragment ions gather along the polarization directions, showing that the molecules are aligned. In addition, comparing the ion intensities in the upper parts and those in the lower parts of the images, one can notice the anticorrelation between the CO⁺ image and the S⁺ image in the middle panel [Figs. 2(c) and 2(d)] and the opposite anticorrelation between the two images in the bottom panel [Figs. 2(e) and 2(f)]. When the relative phase is zero [Figs. 2(c) and 2(d)], the upper part of the CO⁺ image is more intense than the lower part, and the lower part of the S⁺ image is more intense than the upper part. In contrast, when the relative phase is pi [Figs. 2(e) and 2(f)],

the lower part of the CO^+ image is more intense than the upper part, and the upper part of the S^+ image is more intense than the lower part. These results clearly show that the molecular orientation can be changed simply by changing the relative phase between the two wavelengths.

The changes in the fragment yields associated with molecular orientation can also be confirmed by the angular distributions of fragment ions. In Fig. 3, the fragment yields are plotted as a function of θ_{2D} , the projection of the polar angle onto the detector plane. The angles $\theta_{2D} = 0^\circ$ and 180° correspond to the upward and downward directions in the ion images, respectively. The red solid lines show the distributions of CO^+ and the black dotted lines show the distributions of S^+ . One can see that CO^+ is more intense (weaker) than S^+ at around $\theta_{2D} = 0^\circ$ (180°) when the relative phase is zero and that S^+ is more intense (weaker) than CO^+ at around $\theta_{2D} = 0^\circ$ (180°) when the relative phase is π .

The degree of molecular orientation is evaluated by the average of $\cos\theta_{2D}$, $\langle\cos\theta_{2D}\rangle$, defined as

$$\langle\cos\theta_{2D}\rangle \equiv \frac{\int_0^{2\pi} \cos\theta_{2D} f(\theta_{2D}) d\theta_{2D}}{\int_0^{2\pi} f(\theta_{2D}) d\theta_{2D}}, \quad (3)$$

with $f(\theta_{2D})$ the distribution function of the fragment ions observed at the angle θ_{2D} . The value of $\langle\cos\theta_{2D}\rangle = 0$

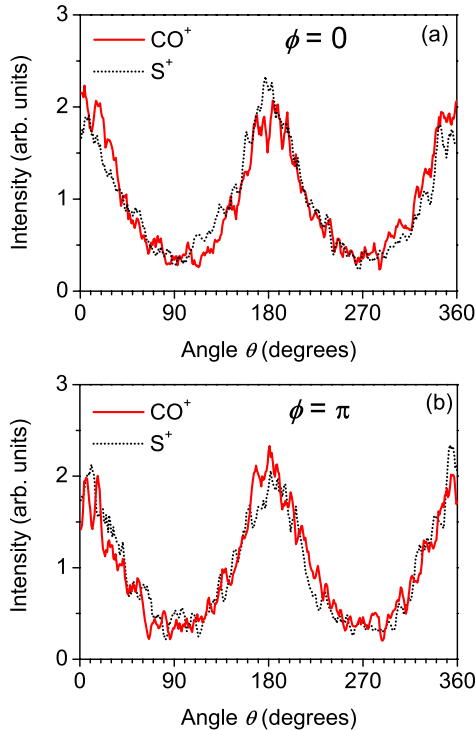


FIG. 3 (color online). The fragment intensities plotted as a function of θ_{2D} , the projection of the polar angle onto the detector plane for the relative phases $\phi = 0$ (a) and $\phi = \pi$ (b). The angles $\theta_{2D} = 0^\circ$ and 180° correspond to the upward and downward directions, respectively, in the ion images shown in Fig. 2. The red solid lines show the distributions of CO^+ and the black dotted lines show the distributions of S^+ .

means that the molecules are randomly oriented or only aligned and the value of $\langle\cos\theta_{2D}\rangle = \pm 1$ corresponds to perfect orientation. Based on the observation of many ion images, we evaluate $\langle\cos\theta_{2D}\rangle$ as a function of the relative phase between the two-color laser fields. The results are summarized in Fig. 4, where the red circles and black squares represent $\langle\cos\theta_{2D}\rangle$ for CO^+ and S^+ , respectively. When $\langle\cos\theta_{2D}\rangle$ is not saturated and proportional to the potential difference between the deeper and shallower wells, $\langle\cos\theta_{2D}\rangle$ is expected to follow $\cos\phi$ [see Eq. (2)]. The red solid and black dotted curves in Fig. 4 are the least squares fits of the observations. One can see that $\langle\cos\theta_{2D}\rangle$ for CO^+ modulates out of phase with that for S^+ and that molecular orientation can be changed every π change in the relative phase between the two-color laser fields. These observations provide conclusive evidence of molecular orientation with an intense nonresonant two-color laser field. The degree of molecular alignment $\langle\cos^2\theta_{2D}\rangle$ defined by replacing $\cos\theta_{2D}$ with $\cos^2\theta_{2D}$ in Eq. (3) is ~ 0.66 irrespective of the change in the relative phase between the two wavelengths. This combined with the fact that the modulations of $\langle\cos\theta_{2D}\rangle$ shown in Fig. 4 can be well fitted by $\cos\phi$ means that the anisotropic hyperpolarizability interaction [the third term in Eq. (2)] is the first-order perturbation to the anisotropic polarizability interaction [the second term in Eq. (2)] under the present conditions.

The advantages of all-optical molecular orientation are multifold; the fact that the technique does not rely on the interaction between the permanent dipole moment and an electrostatic field brings us the first three advantages. (1) Molecular orientation is free from the directional restriction imposed by the electrodes and can be controlled simply by rotating the laser polarization or by changing the relative phase between the two wavelengths. (2) The technique can be applicable even to virtually nonpolar molecules with a very small permanent dipole moment as long as the sample molecule has anisotropic hyperpolarizability as well as anisotropic polarizability. (3) All-optical molecular orientation can be extended to achieve completely

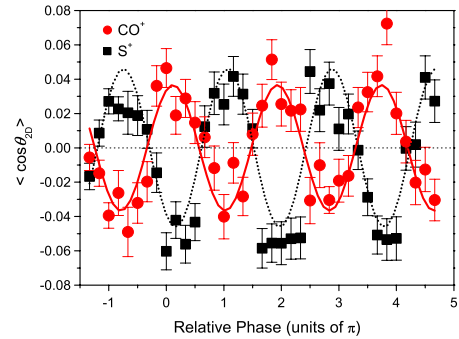


FIG. 4 (color online). The degree of molecular orientation $\langle\cos\theta_{2D}\rangle$ as a function of the relative phase between the two-color laser fields. The red circles and black squares represent $\langle\cos\theta_{2D}\rangle$ for CO^+ and S^+ , respectively. The red solid and black dotted curves are the least squares fits of the observations.

field-free molecular orientation. As a matter of fact, we have proposed a practical and versatile technique to achieve completely field-free molecular orientation with an intense, nonresonant, two-color laser field with a slow turn on and rapid turn off [24]. (4) Since the technique is based on the nonresonant interactions, it is versatile and applicable to various molecules. We have already observed orientation of C_6H_5I molecules with the present technique. (5) The technique can be used to achieve three-dimensional molecular orientation with the polarizations of the two wavelengths crossed [25]. (6) The laser-induced molecular alignment technique has already been used to evaluate polarizability anisotropies of molecules both in the adiabatic regime [26] and in the nonadiabatic regime [27]. Combined with the evaluated polarizability anisotropy of a molecule, the technique of all-optical molecular orientation could be further utilized for the experimental evaluation of hyperpolarizability of molecules based on the fitting between the measured degrees of molecular orientation and the numerical simulations.

For a specific sample molecule, the degree of molecular orientation is determined by the intensity of a two-color laser field and the initial rotational temperature of the molecules. It should be noticed that there is still some room to increase the degree of molecular orientation shown in Fig. 4 by increasing the intensity of the two-color laser field or by lowering the initial rotational temperature of OCS molecules. The use of thermal ensemble as in the present case allows us to utilize a relatively simple experimental setup and to produce molecular beams with significant density, while the increase of the degree of molecular orientation is eventually limited by the incoherent contributions of Boltzmann distributed initial rotational states. On the other hand, if the higher degree of molecular orientation is crucial in some applications, it may be an option to use state-selected molecules which can be prepared by an elaborate hexapole focuser [28] or a molecular deflector [29] though the molecular density will be much reduced. With a sample of state-selected molecules, completely field-free molecular orientation could be achieved even with an intense femtosecond two-color phase-locked laser pulse.

In conclusion, we report the first clear evidence of all-optical molecular orientation with a two-color phase-locked laser field in the adiabatic region. We hope that all-optical molecular orientation will be further developed and contribute to progress in studies on electronic stereodynamics in molecules, stereodynamics in chemical reactions, ultrafast molecular imaging, attosecond science, surface science, selective preparation of one of enantiomers, the development of molecular switches, and so on.

K. O. and M. H. contributed equally to this work. The authors are grateful to Masahiro Muramatsu for his contribution in the early stage of this work. They also thank Akihisa Goban for his fruitful discussions. This work was supported by Grant-in-Aid for Scientific Research (A) No. 19204041 from JSPS, Grant-in-Aid for Specially

Promoted Research No. 21000003 from MEXT, and the Photon Frontier Network Program of MEXT.

Note added.—After the submission of our manuscript, Ref. [30] was published. It should be noted that higher pump pulse intensities and the probe pulse polarization parallel to the pump pulse polarization are used in their observations.

*hsakai@phys.s.u-tokyo.ac.jp

- [1] H. Stapelfeldt and T. Seideman, *Rev. Mod. Phys.* **75**, 543 (2003).
- [2] T. Seideman and E. Hamilton, *Adv. At. Mol. Opt. Phys.* **52**, 289 (2005).
- [3] I. V. Litvinyuk *et al.*, *Phys. Rev. Lett.* **90**, 233003 (2003).
- [4] T. Suzuki, S. Minemoto, T. Kanai, and H. Sakai, *Phys. Rev. Lett.* **92**, 133005 (2004).
- [5] D. Zeidler *et al.*, *Phys. Rev. Lett.* **95**, 203003 (2005).
- [6] S. Minemoto, T. Kanai, and H. Sakai, *Phys. Rev. A* **77**, 041401(R) (2008).
- [7] J. Itatani *et al.*, *Nature (London)* **432**, 867 (2004).
- [8] T. Kanai, S. Minemoto, and H. Sakai, *Nature (London)* **435**, 470 (2005).
- [9] T. Kanai, S. Minemoto, and H. Sakai, *Phys. Rev. Lett.* **98**, 053002 (2007).
- [10] B. Friedrich and D. R. Herschbach, *Nature (London)* **353**, 412 (1991).
- [11] H. J. Loesch and A. Remscheid, *J. Phys. Chem.* **95**, 8194 (1991).
- [12] V. A. Cho and R. B. Bernstein, *J. Phys. Chem.* **95**, 8129 (1991).
- [13] B. Friedrich and D. Herschbach, *J. Phys. Chem. A* **103**, 10280 (1999).
- [14] H. Sakai *et al.*, *Phys. Rev. Lett.* **90**, 083001 (2003).
- [15] S. Minemoto *et al.*, *J. Chem. Phys.* **118**, 4052 (2003).
- [16] H. Tanji, S. Minemoto, and H. Sakai, *Phys. Rev. A* **72**, 063401 (2005).
- [17] Y. Sugawara, A. Goban, S. Minemoto, and H. Sakai, *Phys. Rev. A* **77**, 031403(R) (2008).
- [18] A. Goban, S. Minemoto, and H. Sakai, *Phys. Rev. Lett.* **101**, 013001 (2008).
- [19] T. Kanai and H. Sakai, *J. Chem. Phys.* **115**, 5492 (2001).
- [20] M. J. J. Vrakking and S. Stolte, *Chem. Phys. Lett.* **271**, 209 (1997).
- [21] C. M. Dion *et al.*, *Chem. Phys. Lett.* **302**, 215 (1999).
- [22] S. Guérin *et al.*, *Phys. Rev. Lett.* **88**, 233601 (2002).
- [23] O. Atabek, C. M. Dion, and A. B. H. Yedder, *J. Phys. B* **36**, 4667 (2003).
- [24] M. Muramatsu, M. Hita, S. Minemoto, and H. Sakai, *Phys. Rev. A* **79**, 011403(R) (2009).
- [25] N. Takemoto and K. Yamanouchi, *Chem. Phys. Lett.* **451**, 1 (2008).
- [26] S. Minemoto, H. Tanji, and H. Sakai, *J. Chem. Phys.* **119**, 7737 (2003).
- [27] D. Pinkham, T. Vogt, and R. R. Jones, *J. Chem. Phys.* **129**, 064307 (2008).
- [28] O. Ghafur *et al.*, *Nature Phys.* **5**, 289 (2009).
- [29] L. Holmegaard *et al.*, *Phys. Rev. Lett.* **102**, 023001 (2009).
- [30] S. De *et al.*, *Phys. Rev. Lett.* **103**, 153002 (2009).